Appl. Phys. B 68, 1073–1083 (1999) / DOI 10.1007/s003409900055

Applied Physics B
Lasers
and Optics

Real-time holographic interferometry using sillenite photorefractive crystals. Study and optimization of a transportable set-up for quantified phase measurements on large objects

M.P. Georges, Ph.C. Lemaire

Centre Spatial of Liège - Université de Liège, Parc Scientifique du Sart Tilman, Avenue du Pré-Aily, B-4031 Angleur, Belgium
(E-mail: mgeorges@ulg.ac.be)

Received: 4 December 1998/Revised version: 6 March 1999/Published online: 12 April 1999

Abstract. We present the development of a holographic interferometer that uses a photorefractive crystal of the sillenite family as holographic recording medium. The aim of this work is to achieve a transportable and breadboard instrument, with a flexible design and which is user friendly for the quantified measurements of displacements on large scattering objects. The state of the art of the use of photorefractive crystals in holographic interferometry is presented. Based on the latter, a method that is the best suited to our mentioned objectives is chosen: the real-time interferometric technique associated with the crystal configuration exhibiting diffraction anisotropy. On this basis, we have studied and compared two imaging systems, we have experimentally determined the holographic figures of merit of three sillenite crystals samples, and, finally, we have shown the use of two measurement quantification methods. The result of these investigations is a certified and transportable holographic camera prototype containing all the necessary equipment for its operation, which can be easily adapted to various applications. Among these, we show its use in the detection of defects in composite structures, in the measurement of time-evolving deformations, and in the measurement of vibration modes.

PACS: 42.40.Kw; 42.40.My; 42.70.Nq

Holographic interferometry (HI) [1, 2] is a powerful optical method for the observation of micrometric displacements of opaque scattering or transparent objects. In the past, numerous studies have shown that the photorefractive crystals (PRCs) [3, 4], and particularly those belonging to the sillenite family (BSO ($Bi_{12}SiO_{20}$), BGO ($Bi_{12}GeO_{20}$), and BTO ($Bi_{12}TiO_{20}$)), are attractive media for holograms recording in HI [4, 5]. In these crystals, a migration of electric charges appears between illuminated and dark zones that result from the interference between reference and object beams. After charges are trapped in defects of the dark zones, a space-charge field is created that modulates the refractive index through the linear electro-optic effect, yielding phase hologram recording. This process is dynamic and reversible and can take place under the diffusion process (diffusive regime) or under an external electric field (drift regime). The originality of a holographic interferometer that uses such materials is that it simultaneously satisfies two essential features for applied metrological instruments: the in situ self-processing of the recording medium and its indefinite reusability. One can then envisage holographic cameras that are as stand-alone and user friendly as competing methods (speckle interferometry, TV holography [1, 2]) but have higher measurement dynamics and resolution and lower noise levels. In spite of these major advantages, experimental prototypes of PRC interferometers have for long been confined to optical laboratories. This is essentially due to classical drawbacks of PRCs (energetic sensitivity, weak diffraction efficiency, and optical dimensions of crystals) which induced the need for powerful cumbersome lasers and limit the required flexibility of these instruments. The recent availability of much larger good-quality sillenite crystals, powerful compact lasers, and sensitive commercial CCD cameras, has allowed us to overcome these difficulties.

The purpose of this paper is to show a broad study whose achievement is a breadboard holographic interferometer using a sillenite PRC. The required features of the instrument are that (i) it has to be transportable (i.e. a breadboard that includes all the necessary equipment for its utilization), (ii) it has to allow the observation of opaque scattering objects with medium to large dimensions (a typical 50 cm × 50 cm observed area is assumed), (iii) it has to be simple to use (the fewest adjustments possible), (iv) it has to easily give interpretable results (use of phase quantification techniques), and (v) it has to be sufficiently versatile to be adapted to different kinds of applications in HI.

Concerning the holographic technique, three main methods exist. In real-time HI (RTHI) only one hologram is recorded. At the readout step, the object is still illuminated and one observes the interference pattern (interferogram) resulting from the superimposition of the wavefronts diffracted by the hologram and the one coming directly from the object (transmitted through the hologram). Each object variation is then observed

Dedicated to Prof. Dr. Eckard Krätzig on the occasion of his 60th birthday and for his outstanding work in the research on photorefractive materials.

directly (*live fringes*). The double-exposure HI (2EHI) requires the recording of two holograms. A further readout step shows the superimposition of both stored wavefronts (*frozen fringes*). A third technique is applied for the case of vibrating objects: the time-average HI (TAHI). The hologram is recorded during the vibration of the object and over a longer time than the vibration period. The metrological need in today's applications is not limited to qualitative evaluation of displacements but requires a quantification of these. Generally, in RTHI and 2EHI, the interferogram is written in each point (x, y) of an observation plane as

$$I(x, y) = I_{\text{average}}(x, y)\,[1 + m(x, y)\cos(\phi(x, y))]\ , \qquad (1)$$

with $I_{\text{average}}(x, y)$ the average intensity and $m(x, y)$ the contrast. The quantity $\phi(x, y)$ is the phase difference between both transmitted and diffracted wavefronts and is related to the searched displacement of the object surface. For this purpose, phase-quantification methods [1, 2, 6] are considered in all modern interferometric tools, leading to acccurate displacement measurements. These methods allow us to retrieve a phase image $\phi(x, y)$ from the intensity image (1). The displacements are calculated on the basis of the wavelength used and the geometry of the illumination and observation [1, 2]. The two most widespread methods are the phase-shifting (PS) and the Fourier-transform (FT) methods. In PS, the phase is calculated from several interferograms of the same object displacement with a phase shift between each other, whereas with the FT method, it is calculated from a single interferogram in which a carrier fringe pattern has been added before acquisition. The first one is generally more accurate but requires stability during the PS process, whereas the second one can be used with dynamic phenomena.

Pioneering experiments in HI with PRCs have been carried out by the group of Huignard. They proposed first the 2EHI in BSO for observing phase variations in transparent objects [7] and TAHI for vibration-modes visualisation [8, 9]. Later they showed the use of energy transfer applied to TAHI [10]. The largest objects studied in these early works was a 20 cm × 20 cm plate under vibration and with the TAHI as shown by the same group [11] using an electric field applied to the crystal and the mobile grating technique in order to enhance the diffracted signal. Very good contrast interferograms were obtained. In 1985, Kamshilin and Petrov [12] proposed for the first time the use of the anisotropy of diffraction applied to the TAHI with a BSO at 514 nm and a BTO at 633 nm. In this configuration, for a particular orientation of the recording beam polarizations, that of the diffracted beam is perpendicular to the input polarization. The diffracted beam can then be filtered from the unwanted transmitted component. This principle was successfully used later by Troth and Dainty [13] who showed high-quality interferograms with 2EHI and TAHI in BSO at 514 nm. After those demonstration of capabilities of PRCs in HI, relevant works concerning the optimization of holographic interferometers have been carried out by Troth et al. [14] and Miridonov et al. [15] on the basis of the promising diffraction anisotropy scheme. From radiometric considerations, Troth et al. [14] concluded that objects of typically 1 m^2 could be monitored with BSO crystals and a laser of 1 W.

Recently, some groups have focused their works on the development of instruments for applications in industrial fields. They all aim to perform quantitative measurements on scattering objects. The group of von Bally has developed a holographic camera that records a sequence of double exposures [16, 17]. It is based on a BTO crystal and works with an argon laser at 514 nm. The phase calculation is performed either by FT [16] or by PS [17]. The method used is 2EHI which leads to high intensities on the crystal in order to have short recording times, small objects positioned close to the holographic head are examined. Recently they showed the use of pulsed illumination with the FT technique for phase quantification [18, 19]. Pouet and Krishnaswamy [20] proposed the use of 2EHI associated to a stroboscopic technique for the visualisation of vibration patterns with a BSO at 514 nm. Once again short response times are needed so relatively small objects are observed. The group of G. Roosen proposed the use of a special polarization separation technique for obtaining simultaneously two phase-shifted images of the same object displacement [21]. They can perform quantitative phase measurement with high accuracy based on a single shot. Their holographic camera is breadboarded and has been successfully used in cw at 514 nm and was further used in pulsed illumination with a ruby laser (694 nm) [22]. In the last case, the wavelength is badly adapted to the sensitivity range of the sillenite crystal. For that reason, a BGO-doped copper crystal has been especially developed for increasing the response at these wavelengths. Though the response is weak in these conditions, the quality of the results is acceptable. This is the first use of pulsed illumination with a PRC on an industrial example (turbine blade under vibration).

The present paper is concerned with the development of a breadboard holographic interferometer using a sillenite crystal under the configuration of diffraction anisotropy associated to the RTHI technique. In Sect. 1, we motivate the choice of this combination, we briefly present a first preliminary experiment that has led us to a more systematic study. In Sect. 2, we present the main instructive results of the study and optimization of the breadboard interferometer for the observation of large objects displacements. Two axes of work are considered: the imaging system and the sillenite samples used. In Sect. 3, we discuss the use of two phase-quantification methods, the PS and the FT, especially we point out the particularities of the PRCs, either leading to errors in the final results, or bringing some limitations that have to be circumvented. Concerning this particular point, our purpose here is to produce phase images $\phi(x, y)$, we omit the final displacements calculation. In Sect. 4, we show numerous applications, mainly grouped in three categories: the static, the dynamic (non-vibratory), and the vibratory displacements.

1 Choice of the method and presentation of the study

The method used is the RTHI associated with the crystal configuration exhibiting anisotropy of diffraction. In the case of RTHI, the polarizer at the output of the crystal is used to equalize the intensities of the transmitted and the diffracted waves, which is the basic condition for an optimization of the interferogram contrast. In this configuration, once the necessary polarizers are correctly orientated, there is no further adjustment needed, which copes with the "ease-of-use" con-

dition. Also, no electric field is applied to the crystal in order to optimize the anisotropy of diffraction and to have a maximum diffraction efficiency for large angles between reference and object beams [4]. This geometrical configuration allows the use of short-focal-length optics close to the crystal without being disturbed by the reference beam. This also has positive consequences concerning the intensity of light scattered by objects on the crystal and the set-up compactness by placing the objects close to the holographic head. The choice of the RTHI technique is justified by the fact that it is a priori open to more applications than other techniques (2EHI and TAHI). Indeed, static, dynamic, and vibratory displacements can be examined in RTHI. In the case of vibrations, a stroboscopic technique is associated [23]. 2EHI can be used also in all cases but is more complicated in the case of the dynamic (continuously evolving) displacements because sequences of double-exposed holograms must be related to one another, which necessitates multiplexing procedures. Finally, phase-quantification techniques are more complicated to introduce with 2EHI, the PS process requiring the use of a double-reference scheme [17]. TAHI is only applicable to vibrating objects so basically it is too limited. Also, phase-quantification techniques are generally addressed to sinusoidal fringe patterns, which is not the case in TAHI (Bessel-fringe profiles).

On the basis of this choice, a first set-up has been developed with a BSO crystal (1 cm × 1 cm of optical face and 3 mm thick) and is presented elsewhere [24]. It used a non-transportable argon laser and was intended to be the starting point of a more systematic study for the building of a transportable system. Due to the weak diffraction efficiency in diffusive regime, the CCD camera has to be sufficiently sensitive. A single objective lens attached to the CCD observes the object and has been chosen following geometric and radiometric considerations. From the radiometric point of view, the object has to be sufficiently close to the crystal. An important fact to point out is the following. When dealing with large scattering objects at a large distance from the holographic head, generally the object beam intensity is much weaker than the reference intensity at the level of the crystal. For PRCs, this has a consequence that the diffracted intensity is proportional to the object beam intensity at the crystal level. It follows that it has to be high enough to give a diffracted intensity detectable by the CCD camera, taking into account the global transmission of the optical system (lenses, crystal, and polarizers). Moreover, the response time being conditioned by the total intensity of the beams incident on the crystal, it is possible to adjust it by changing the reference beam intensity without affecting the diffracted intensity. Nevertheless the noise increases in the same way as the reference beam intensity, as noted in [13–15], and a compromise has to be found between short response time and high SNR of interferograms.

With an argon laser emitting 2.2 W at 514 nm, the combination that has given the best results is the one where the object is illuminated with 2.2 W and placed at 1.2 m from the objective lens (26 mm focal length, 1.1 aperture). The observed area is of 30 cm × 20 cm. The intensity of the object beam is 8 $\mu W/cm^2$ at the crystal input and is about 30 times smaller than that of the reference beam. Excellent-quality interferograms were obtained in non-destructive testing with this instrument [24].

Following this first preliminary experiment, a systematic study has been carried out. It is presented in the next two sections. First, the optimization of the breadboard optical set-up, mainly divided in two axes: (i) the optimization of the imaging system in order to increase the ratio between the object area observed and the available laser power, and (ii) determine the performances of different sillenite PRCs within the set-up. Second, the validation of phase-quantification methods with such an interferometer. This consists of studying the influence of the use of PRCs with the phase-quantification methods.

2 Study and optimization of the interferometer

2.1 Study of the imaging system

The scope of this study is to optimize the ratio of the observed area to the illumination power. For that purpose, the solution is to set the object as close as possible to the optical head. This implies the use of large crystals to avoid vignetting effects by the crystal itself: the largest sillenite samples that can be obtained with good optical quality have windows of typically 3 cm × 3 cm. Two optical systems were studied with such crystals and their performances compared. The only constraint was that they have to observe the same object area and that the luminous intensity coming from the object at the level of the crystal is the same for both systems. The first system (system 1) uses a single objective lens after the crystal, with a short (16-mm) focal length (f.l.) and the object is set at 1.3 m from the optical head. It is similar to the one used in [24] but with a large crystal instead. The second system (system 2) uses two objective lenses: a first one (frontal objective, 50 mm f.l.) images the object upon the crystal and the second one (relay objective, 26 mm f.l.) images the intermediate image onto the CCD. In this case, the object is closer to the optical head: 1 m. Figure 1 shows the breadboard instrument with the second system.

In regard to what is known from the preliminary experiment [24], an object beam intensity at the crystal input of typically 10 $\mu W/cm^2$ is considered as a basic level for our study. Taking this into account and with the imaging parameter mentioned above, both systems achieve the same field of view (55 cm × 37 cm) but the second system requires only 340 mW to illuminate the object whereas the first one requires 2 W.

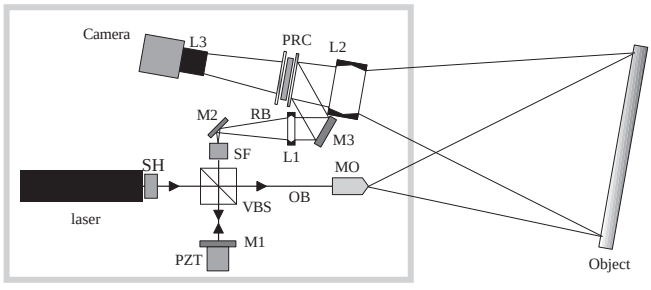

Fig. 1. Breadboard holographic interferometer. SH: shutter; VBS: variable beamsplitter; OB: object beam; MO: microscope objective; PZT: piezoelectric translator; SF: spatial filter; M1, M2, M3: mirrors; RB: reference beam; L1: collimation lens; L2, L3: objective lenses; PRC: photorefractive crystal between two polarizers

Both optical schemes were experimentally compared: their respective response (diffracted, transmitted, and diffusion intensities) were measured and the interferometric quality was deduced (average intensity and contrast of interferograms). Detailed discussions are given in [25, 26], here we summarize the main instructive results.

Principally, three waves arrive at the CCD plane: the transmitted object wave, the diffracted wave, and the scattering noise. The last can have several origins: imperfections in the crystal volume, scratches or dust at the surface of the crystal, or any other optical element. Some authors impute it to birefringence induced by stresses [13]. The measurement of the intensities described above has been performed with the complete instrument shown in Fig. 1 but including each optical system in its turn. In order to measure correctly the diffracted intensity, the transmission axis of the polarizer after the crystal is set in the direction of the diffracted polarization, i.e. crossed with respect to the transmitted wave polarization. An important fact for these experiments is that the measurements were performed with the complete instrument and the object considered is a large white coated plate. One can then say that the results will be representative of the instrument behaviour in realistic working conditions. The laser is the argon (514 nm) and the crystal a BGO:Cu whose origin and dimensions will be given in Sect. 2.2. The CCD camera has been replaced by a silicium photodetector. For several values of the reference intensity I_{ref}, we monitor the diffracted signal during a recording/readout sequence. During the recording step, the intensity evolution with the time t is of the type

$$I = I_{t,\text{res}} + I_{n,\text{res}} + I_{\text{diff}}^{(\text{sat})}\left[1 - \mathrm{e}^{-t/\tau}\right]^2 , \qquad (2)$$

with $I_{t,\text{res}}$ and $I_{t,\text{res}}$ the residual intensities of the transmitted and the noise waves; $I_{\text{diff}}^{(\text{sat})}$ is the saturation value of the diffracted intensity and τ the response time.

A series of measurements has been performed for different values of I_{ref} and the recording curves are fitted by the third term of (2) where $I_{\text{diff}}^{(\text{sat})}$ and τ are the free parameters. Figure 2 shows the diffracted intensity at saturation $I_{\text{diff}}^{(\text{sat})}$ for both systems in function of the reference beam intensity. It is seen that when the readout intensity increases, $I_{\text{diff}}^{(\text{sat})}$ increases up to a certain level, after which it no longer evolves. This is contrary to the behaviour expected: the diffracted intensity is proportional to the incident intensity and does not depend on the reference beam intensity. The explanation is that, for small values of I_{ref}, the response time is so long that the holographic recording does not complete up to saturation in a correct way because of the environmental perturbations. Note that care was taken to limit this problem (optical table with table top, no operator in the vicinity of the experiment during measurement). These ideal conditions are used because we want to analyze the instrument behaviour without being disturbed by external perturbations. Of course, under practical working conditions, the performances are degraded when perturbations increase. The smaller values of the diffracted intensities obtained with system 2 are explained by the fact that some vignetting is present with this system due to the two-objective lenses scheme, this effect is not due to the crystal. The vignetting is mainly present in the edges of the field and is seen in this kind of measurement because a large photodetector is used. From the same measurements, we deduce the residual intensities [25, 26]. We naturally found that the noise

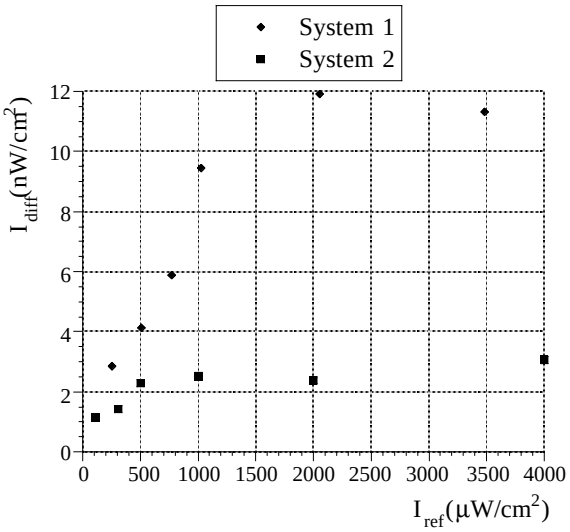

Fig. 2. Diffacted intensities of the waves detected in the image plane as a function of the reference intensity, for both imaging systems and with the output polarizer orientated along the diffracted polarization

intensity is proportional to the incident readout intensity, as already observed by Miridonov et al. [15]. We also deduced the response time for each system and determined a working point taken as the minimum value of I_{ref} at which the holographic recording is well completed, i.e. $I_{\text{diff}}^{(\text{sat})}$ has a stable value. This value is about 1 to 2 mW/cm^2 and appears to be independent of the angular discrepancies existing between both systems for the object beam.

At this working point, the interferogram quality (average intensity and contrast) was experimentally deduced. A model has been developed [25, 26] and the calculated values were compared to values measured in interferograms. It is found that the interferogram quality is slightly smaller (contrast m of typically 0.5) with the system 2 than with system 1 ($m = 0.9$), principally due to the fact that the scattering noise is higher in that case. This is obvious because in system 2 the crystal and polarizers (and their imperfections, scratches, and dust) are in the vicinity of the intermediate image plane. Nevertheless it has a negligible influence on the final results (quantified phase calculated after PS), as is shown in [25, 26].

From this part of the study, we conclude that the second system is the best solution for a transportable breadboard, because a smaller laser power is necessary than for the first system, allowing the use of a small transportable laser source (a 400-mW diode-pumped frequency-doubled YAG laser is sufficient for the surfaces considered). Also the object is closer to the holographic head, which is more comfortable in practice if large objects are studied. Finally, the interferogram quality is still found to be very good.

2.2 Study of the crystals

After having chosen an optical imaging system, it is interesting to see which sillenite crystal gives the best performances. It was then advisable to compare species that can be obtained in large optical windows, say BSO and BGO crystals. The sample we considered are described in Table 1. Both BGOs are grown by Dr. J-C. Launay at the Institut de Chimie de

Table 1. Dimensions and origin of the sillenite crystals in comparison

	Width /mm	Height /mm	Thickness /mm	Origin
BSO	30	30	2.5	Castech (Ch)
BGO	37	30	2.5	ICMCB (Fr)
BGO:Cu	29	27	2.6	ICMCB (Fr)

la Matière Condensée (ICMCB) of the Bordeaux University (France) and the BSO comes from Castech (China).

The crystals are antireflection-coated in order to limit the losses by reflection which can be of the order of 35%. The same kind of measurement (intensities of waves arriving on the CCD, the response times, the interferogram quality) were performed in the complete instrument with imaging system 2 and under practical realistic conditions, the same used for the previous part of the study (Sect. 2.1). Also, these properties are measured for two useful wavelengths: 514 nm (argon laser) and 532 nm (YAG laser). The results at 532 nm have already been presented briefly [27]. Complete results appear in [25].

Before performing these measurements, we have to determine the optimum angle (or equivalently the fringe spacing) to use between the recording beams. The crystal is illuminated by two plane waves at 514 nm, the ratio between beams on the crystal is 1, which maximizes the diffraction efficiency and a 633-nm He-Ne probe beam monitors the hologram build-up. $I_{\text{diff}}^{(\text{sat})}$ and τ are deduced from these measurements as a function of the fringe spacing [25, 27] and one chooses a value of the latter such that the crystal has an optimum response, say a compromise between the highest diffraction efficiency and the shortest response time. The angles found are not the same for the different species and are a function of the wavelength: they range between 40° and 52°.

Using the optimum values of the angle between beams, the intensities of the beams present at the CCD plane were measured as a function of the reference intensity. The behaviour of $I_{\text{diff}}^{(\text{sat})}$ as a function of I_{ref} is similar to what is shown in Fig. 2. We observed that the BGO:Cu is the most efficient and the BSO the least. It has to be noted that the BSO shows a high residual birefringence in a large part of the crystal, as well as weak diffraction from the same zone. For that reason we cannot conclude that the BSO is a priori a bad candidate, but from the diffraction point of view, this sample is not satisfactory.

Figure 3a,b shows the measured values of the response times as a function of I_{ref} for all crystals at 514 nm and 532 nm. In order to correctly interpret the results, one has to keep in mind that the response time depends on the angle and that is different for each crystal and because the choice of this angle results from a compromise between diffraction efficiency and response time. Obviously, τ is inversely proportional to the intensity and the BSO is the fastest of all. BGO and BGO:Cu have an equivalent response time at 514 nm but the BGO:Cu is faster at 532 nm.

The interferograms contrast and average intensity can be determined in the same way as in Sect. 2.1. Values of these quantities were computed from a model and compared to values measured on interferograms, showing good agreement between each other [25, 27]. In the case of BSO, poor contrast values, as well as spatial variations of the contrast, are observed due to its spatially inhomogeneous photorefractive response. The BGO:Cu gives the best interferogram quality.

Following the above results, we have chosen the BGO:Cu crystal for the breadboard because it gives the better compromise between efficiency, response time, and interferometric quality at 532 nm, which is the wavelength of the transportable laser that will be considered in the prototype. The working point considered ($I_{\text{ref}} = 2\ \text{mW/cm}^2$) at 532 nm gives a response time of about 9 s.

3 Study of phase-quantification techniques

3.1 Phase-shifting

3.1.1 Preliminary remarks. The phase-shifting is introduced during the readout by translating a mirror in the reference beam by means of a piezoelectric transducer (PZT in Fig. 1), the consecutive interferograms are then stored after each phase step. The interferograms I_k are written

$$I_k = I_{\text{average}}\,[I + m\cos(\phi + \beta_k)]\ , \tag{3}$$

with $k = 1, ..., N$ (N integer and greater or equal to 3) and the phase step β_k. In this expression, the dependency of the different quantities in (x, y) has been omitted. Since the acquisitions are delayed in the time, we refer here to the "temporal PS", in contrast to the "simultaneous PS" performed by several cameras at the same instant (such as in the instrument developed by Labrunie et al. [22]). The computation of

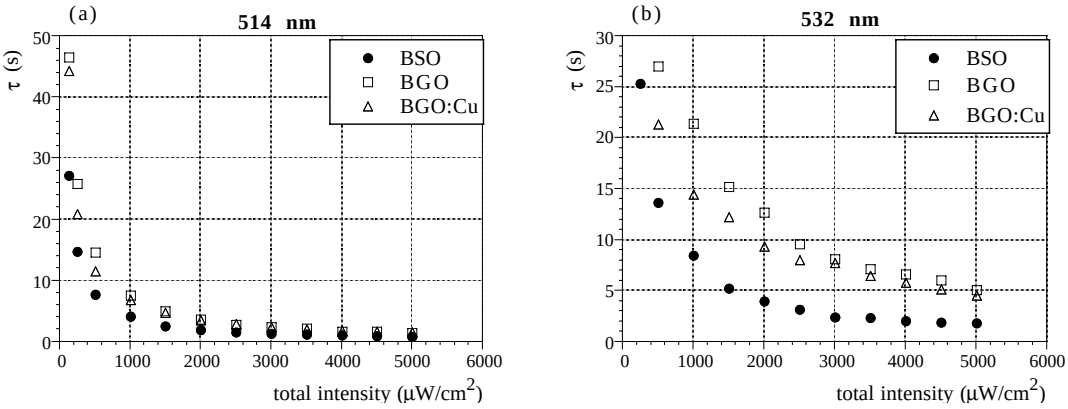

Fig. 3a,b. Response time of all crystals at 514 nm (**a**) and at 532 nm (**b**)

phase is carried out following one or other algorithm depending on the number N and the value of the additional constant phase β_k at each step [2]. Generally, the latter is a fraction of 2π (calibrated phase-steps) but we use the algorithm of Carré ($N = 4$) that does not require calibrated steps, provide they are equal between each consecutive interferograms. This has several advantages as explained in [24]. The phase calculated by the Carré algorithm is given by

$$\phi_{\text{calc}} = \tan^{-1}\left(\frac{\{(I_1 - I_4 + I_2 - I_3)[3(I_2 - I_3) - (I_1 - I_4)]\}^{1/2}}{(I_2 + I_3) - (I_1 + I_4)}\right). \tag{4}$$

In [24], we already have studied the errors on the calculated phase. A particular error arises in PRC-based interferometers from the hologram erasure during the readout, with the consequence that the interferogram disappears. The first approach followed in [24] takes into account only the decrease of the interferogram contrast m. This approach is valid provided the interferogram acquisition is fast compared to the photorefractive response time. Indeed, an important condition to apply PS is that the N interferograms I_k have the same average intensities and contrasts, which is not certain here.

The general method to determine the error the PS process introduces in the calculated phase is the following. The interferograms are simulated by injecting in (3) the values of I_{average}, m, β_k, and the phase ϕ. For the latter, one generates a series of values linearly increasing from 0 to 2π. The simulated interferograms are then injected into (4). The comparison between the calculated phase ϕ_{calc} and the initial phase ϕ gives the error due to the PS process. Generally one considers the peak-to-valley (PV) or the root-mean-square (RMS) errors, the latter being preferred because it does not take into account local errors. In the procedure described above, one can now introduce different perturbing phenomena. This has been carried out in [24] in which the influence of several common error sources was analyzed, among which the environmental perturbations being the more important. A final error of $\lambda/40$ (RMS) was found in the object displacement measurement mainly coming from the external perturbations. As mentioned above, an error comes from the photorefractive erasure of the hologram, we will call it the photorefractive error and it is described hereafter.

3.1.2 Photorefractive error. Here we consider a more complete model that combines the variations of the average intensity and the contrast and takes into account the rise of secondary holograms. As a matter of fact, between the instant at which the hologram is read out and the instant at which it is completely erased (the new hologram is recorded at saturation), both holograms exist. As a consequence, a double-exposure interferogram appears and is competing against the real-time interferogram. If a phase step β is applied, the new hologram will stop its recording and immediately begin to decrease. Once the step is applied, a third hologram will be recording, and so on until the last phase step. Figure 4 shows the situation where four interferograms are stored at instants t_0, t_1, t_2, and t_3. One also considers that the phase steps are discrete and that the time interval $\Delta t = t_{i+1} - t_i$ is constant.

We can calculate analytically the four interferograms used in the PS process by considering the superimposition of the

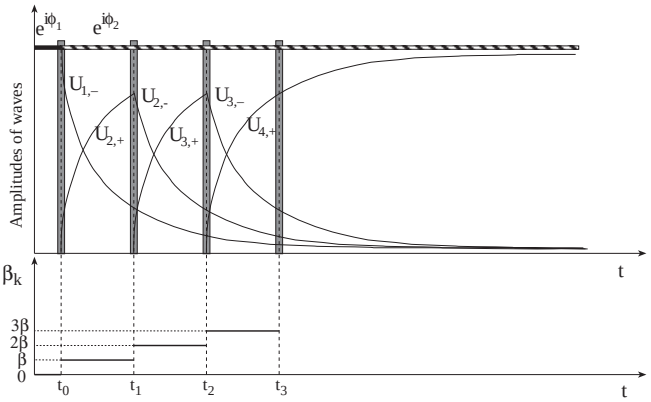

Fig. 4. Amplitude of the transmitted and diffracted waves during the PS sequence. The phase steps are multiple of a quantity β

amplitudes of all waves present at the instants of image capture (grey rectangles in Fig. 4). In all cases, the transmitted wave is present: first object state before instant t_0 (black horizontal line) followed by the second object state after t_0 (dashed horizontal line). The phases associated to this wave before and after t_0 are, respectively, ϕ_1 and ϕ_2. At each capture instant, several wave fields are coherently superimposed. At t_0, only the diffracted wave ($U_{1,-}$ with a phase ϕ_1) and the transmitted wave (phase ϕ_2) are present. The intensity of the first interferogram I_1 is then easily calculated by multiplying the total field amplitude by its complex conjugate. At other capture instants, one has to take into account other components that increase with the time until a new phase step is applied ($U_{n,+}$ with $n = 2, 3, 4$), as well as components that decrease ($U_{n,-}$ with $n = 1, 2, 3$). The analytical expressions of I_1, I_2, I_3, and I_4 are detailed in [25].

The discussion on the error is based on the temporal parameters Δt and τ. Intensities I_1 to I_4 are inserted into (4). Figure 5 shows the error (in rad) in the calculated phase as a function of the parameter $\tau/\Delta t$.

If we consider the response time $\tau = 10$ s (a typical value of our working point $I_{\text{ref}} = 2\,\text{mW/cm}^2$ and the BGO:Cu crystal at 532 nm) and a Δt of 0.2 s in our phase-shifting process, the error is 0.022 rad, say $\lambda/580$ RMS. When the contribu-

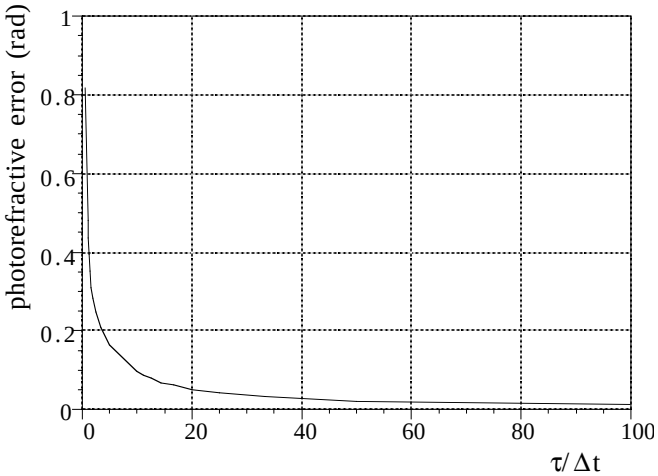

Fig. 5. Photorefractive error as a function of the temporal parameter $\tau/\Delta t$

tion of secondary holograms is suppressed, one obtains $\lambda/730$ RMS. This shows that the parasitic double-exposure interferograms are of little importance with respect to the real-time contribution.

Anyway the photorefractive error found at the used working point and with a fast interferogram acquisition is negligible compared to the error coming from external perturbations ($\lambda/40$).

3.2 Spatial carrier technique with Fourier-transform filtering

This technique requires the addition of a carrier fringe pattern in the interferogram just before the readout. One generally expresses the interference as

$$I = I_{\text{average}} \left[1 + m \cos(\phi + 2\pi f_0 x)\right] , \tag{5}$$

with f_0 the carrier frequency. The Fourier spectrum of (5) shows a central peak with two symmetrical sidelobes. These contain the information on ϕ. One of them is filtered and translated to the origin of the Fourier plane, afterwards it is Fourier-transformed inversely. The imaginary and real parts of the results are used to retrieve ϕ [2, 6]. Contrarily to the PS, the FT requires only one interferogram for the calculation of ϕ, but it has to be noted that there are severe constraints on the spectra of I_{average}, m, and ϕ with respect to the carrier frequency f_0 in order to have no ambiguity in the final result.

Generally the carrier is introduced by tilting the reference beam, leading to the addition of rectilinear fringes. The greater the tilt angle, the higher the carrier frequency. With PRCs, this procedure is not easily applicable because these materials are thick and as a consequence Bragg angular selectivity is important. The latter can be quantified: it is the variation $\Delta\theta_{1/2}$ of the angle around the Bragg angle for which the diffraction efficiency is half its maximum value [28]. It can be shown that $\Delta\theta_{1/2} \approx \Lambda/2d$, with Λ the fringe spacing and d the crystal thickness. In our case, it is about 0.15 mrad. Taking into account that we have to keep a reasonable diffracted signal, this must be reduced to 0.1 mrad. At the level of the image plane, one can calculate that the carrier frequency is about 0.4 fringe/mm, say less than 3 fringes with our CCD camera. Such small carrier frequencies complicate the filtering in the Fourier plane. Nevertheless recent results were shown by others using this technique [18]. In this case, the fact that they work under the drift regime implies that they use smaller angles between recording beams, giving a higher $\Delta\theta_{1/2}$.

In order to overcome this problem, we demonstrated in 1996, for the first time to our knowledge applied to this application, a simple technique [29, 30]. It consists of transversally translating the microscope objective that produces the diverging illumination of the object (see Fig. 1). This illumination can be considered as coming from a point source emitting a spherical wave. The translation occurs after hologram recording at saturation, just before the readout. At the readout, the virtual diffracted image shows the object illuminated by a first point source. The image directly transmitted is illuminated by a new point source. Making abstraction of the hologram, the situation is equivalent to observing the object illuminated by two separate point sources. The fringe pattern resulting from the interference of two point sources is well known: the loci of the interference maxima are a family of revolution hyperboloids whose both foci are the sources. These hyperboloids are intercepted by the object situated at about 1 m from the sources. In principle, the projected fringes have a hyperbolic shape but in practice at such distances, they appear quasi-rectilinear. The typical carrier frequencies, that are used in the examples shown further, are produced by translating the microscope objective of 0.5 mm, introducing around 110 fringes on a 35-cm observed width. The image being digitized on 512 pixels, this leads to typically 4.6 pixels/fringe. When a deformation appears, the number of fringes increases locally. Some interferograms that will be presented in the applications are stored with 3 pixels/fringe, which is close to the Nyquist frequency (2 pixels/fringe).

The phase-calculation errors are different from those found with PS. There is a priori no error arising from the dynamical photorefractive behaviour. The errors come mainly from the parameters of the Fourier filtering. These were already considered by others [6].

4 Applications

4.1 Preliminary remarks

After the global study presented above a transportable breadboard has been built and used in several applications. The final prototype has a size of 80 cm × 30 cm × 20 cm and a weight of 15 kg (cw YAG laser included). The instrument is generally used under moderately stable conditions to allow a proper hologram recording within a few seconds. These conditions can be found in a closed room with a stone table (not necessarily isolated against vibrations), no tabletop is required, and with an operator in the vicinity of the experiment. As discussed above, the error in the measurement is a function of the level of external perturbations. We have to mention that some applications were carried out during the development. We will then indicate which optical system is used in the breadboard and also which laser. Principally the first results were obtained with system 1 and an argon laser of 2.2 W at 514 nm, the more recent (see Fig. 10) are obtained with system 2 and a YAG laser of 490 mW at 532 nm. For the latest obtained (see Fig. 7) concerning a large structure, the system 2 was used with the argon laser.

We must also be clear on the fact that the phase images presented in this chapter result from a straight calculation of the phase, as described in the previous section. There is no filtering of any kind to produce these results.

4.2 Static displacements

The first range of applications is the one of static displacements, when the object is in a new state that does not evolve (or very slowly) with time. This is the simplest case of application and the PS can be easily applied. We already have shown in a previous paper the use of PS on a metallic plate attached on its borders [24]. The deformation was provided by a piezoelectric translator at the rear side of the plate. An example of defect detection in a composite structure was also presented. Here we present new results on a larger field of view (55 cm × 37 cm). The framework is still the detection of

defects in aeronautical composite structures. The defects are of several types: impacts, inclusions, delaminations, etc. System 1 is used and the laser is the argon. The operating mode is the following. The hologram of the object at rest is recorded. Once the storage is completed, both recording beams are shut down in order not to erase the hologram and the object undergoes a stimulation. The latter must be appropriate to the type of structure studied, as well as to the defects searched. Here the stimulation consists of heating the structure with a halogen lamp. After a certain time, the heating is stopped and the object is under relaxation for a few seconds. Afterwards the readout is performed showing an interferogram of the residual deformation, which is sufficiently stable for the PS process. This residual deformation depends on the structure and on the boundary conditions. The defects appear as important local variations in the smoother global deformation. The residual deformation then disappears slowly and the object slightly returns to its initial state.

Figure 6a shows one of the interferogram of the PS sequence and Fig. 6b the phase interferogram modulo 2π resulting from the phase calculation (4). These images illustrate the interest of performing the phase calculation. Indeed, in the interferogram, the average intensity and the contrast are weak at the edges of the field with the consequence that the defects in the bottom of the images are not clearly visible. This problem no longer appears in the phase interferogram.

Some examples of this type have been shown in other papers [30, 31]. Several post-processings can also be used to deliver an image of the defects alone [25], as shown in Fig. 6c. A recent example of measurement has been obtained on a larger object (Fig. 7). The optical head-to-object distance is 2 m, the field of view is about 110 cm $\times$ 75 cm but the zone of interest covers 56 cm $\times$ 75 cm. This time, the instrument includes system 2 and the laser is the argon with a power of 1.5 W. The object consists of two CFRP layers sandwiching a honeycomb structure with several inserts. The purpose of the investigation is to analyze the thermo-mechanics of these inserts. After hologram recording at rest, a heater at the rear side of the structure induces a temperature increase. The increase is slow and during the readout, the PS can be applied. Figure 7a shows the deformation after a few min and 7b after 7 min. The basic hologram is not the same for both measurements. The presence of small inserts is visible in Fig. 7b.

The interferograms presented above are, to our knowledge, the first ones obtained with a PRC-based holographic interferometer on such large objects. The measurement error is typically $\lambda/40$ RMS in the object displacement.

4.3 Dynamic displacements (non-vibratory)

The second applications range consists of studying phenomena that are not stationary. On the basis of RTHI, the only possibility is to perform a sequential readout during the object displacement or deformation. Some works used a $LiNbO_3$ crystal with a storage time longer than that of sillenites and a suitable decrease of the readout intensity allows a high number of readouts [32, 33]. More-sensitive crystals allow the use of 2EHI but multiplexing has to be considered to keep track of the deformation between successive interferograms. For

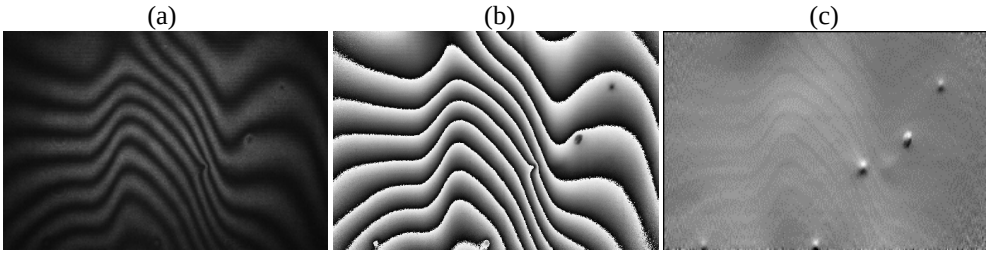

Fig. 6a–c. Detection of defects in an aeronautical composite structure. Basic interferogram (**a**), phase interferogram modulo 2π (**b**), and final defect images (**c**) after phase unwrapping and vertical differentiation. This sample is heated for 5 s by two 500-W halogen lamps, and the relaxation time is 45 s

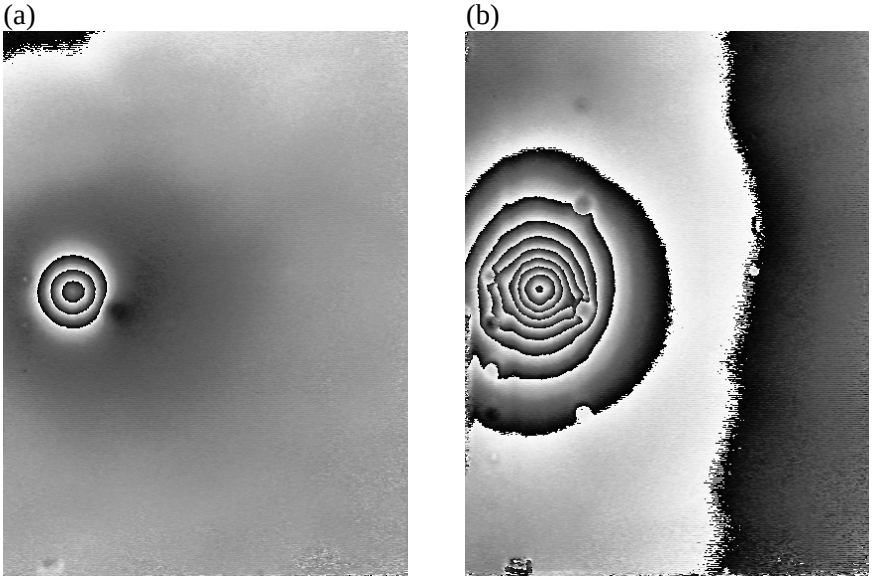

Fig. 7a,b. Deformation of a honeycomb structure with CFRP surfaces under thermal stress by an electric heater at the rear side of the panel. The observed size is 56 cm $\times$ 75 cm. **a** After a few minutes. **b** After 15 min. The presence of inserts is seen in the global deformation fringes

that, the choice of RTHI with sequential readout is interesting because it is simpler to implement. Also it has never been applied to sillenites and we showed its use for the first time in 1996 [29, 30]. Since dynamic interferograms are acquired, PS cannot be applied and we have to use the FT technique which requires only one interferogram for the phase calculation.

The application shown hereafter is the visualization of the deformation of a wooden panel attached at its edges and which is heated by a halogen lamp at the rear side. Due to its thermally insulating property, the deformation can be sufficiently slow and of limited amplitude. This way the measurements will be delayed over a long time and we will be able to appreciate the remanence of the sillenite crystals. The operating mode consists of recording the hologram of the object at rest. Then both recording beams are shut down and the illumination microscope objective is translated. The object stimulation can be initiated and the sequential readout performed. The observed area is 52 cm $\times$ 35 cm but since the fast Fourier transform (FFT) is applied, a square part of 35 cm $\times$ 35 cm is kept and is digitized on 512 pixels $\times$ 512 pixels. Figure 8a shows the interferogram of the deformation together with the carrier fringe pattern, Fig. 8b shows the corresponding Fourier transform (in amplitude). The central peak (zero frequency) contains the spectral information of the average intensity, both conjugate sidelobes contain the information of the wanted phase.

Figure 9 shows phase images (modulo 2π) of a deformation sequence. The first state (Fig. 9a) is observed 20 s after the heating is switched on. It is retrieved from the interferogram shown in Fig. 8. The time interval between consecutive images is 2 min. The duration of each readout is 200 ms. Between two image acquisitions, no light enters the crystal in order to not erase the hologram.

These results show that it is possible to observe a sequence of evolving interferograms. The quality of the resulting phase images is very good but the noise increases in the last ones. This comes from the fact that the interferograms have a contrast that decreases when the number of readouts increases. This implies that the sidelobes tend to be larger and that the window filtering has to be increased. After having translated the filtered sidelobe to the origin of the Fourier plane, higher frequencies are present, which explains the noisier phase images.

The rate of the interferogram acquisition is limited only by the frame grabber. Nevertheless the number of measurements is intrinsically limited by the hologram erasure, due to several factors. First, the dark conductivity, which limits the storage capability of such crystals to a few hours, gives the maximum duration of observable phenomena. The second factor is more crucial: it comes from the erasure during the successive readouts. Here we do not decrease readout intensity for the sake of operational simplicity. It is then most important to strictly limit the opening time of the shutters in the set-up. Taking into account a video frame rate of 25 Hz and considering a response time of about 10 s, one can reasonably record one hundred interferograms. The last factor is the erasure due to parasitic lights that can be limited, even eliminated, by suitable baffling.

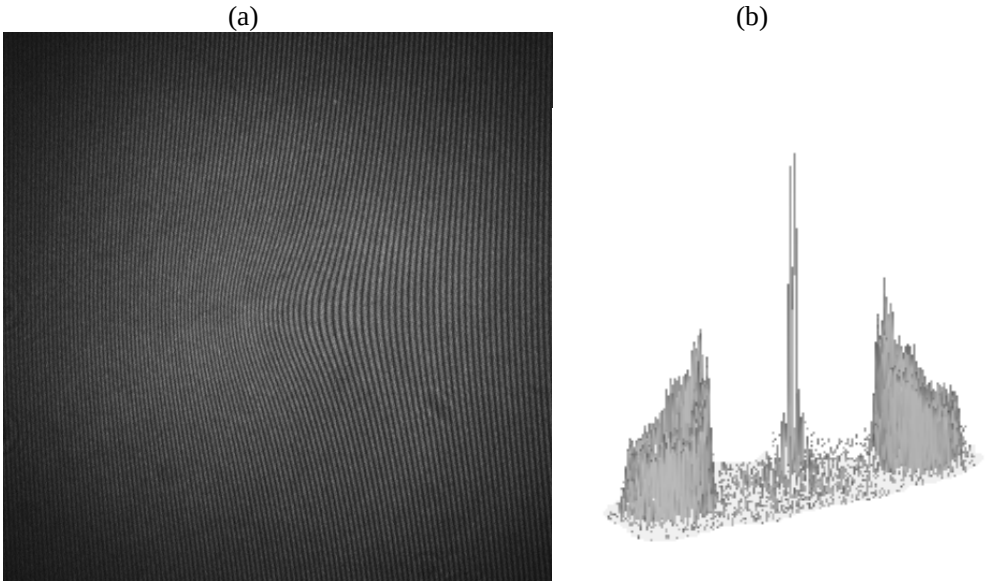

Fig. 8a,b. Interferogram with carrier frequency (**a**) and 3D plot of its Fourier transform (**b**)

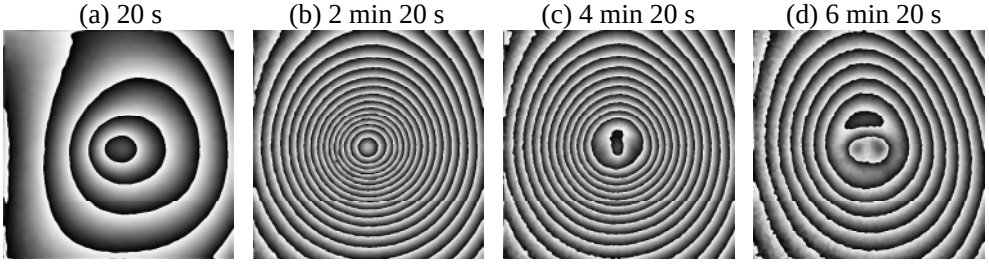

Fig. 9a–d. Phase interferograms modulo 2π showing the deformation of a wooden panel under continuous heating. The time after the beginning of the heating is indicated above each figure

4.4 Vibratory deformations

We have applied the stroboscopic technique to the RTHI for the measurement of vibrations: the hologram of the object is recorded at rest and, when the object is vibrating, stroboscopic readout is performed in synchronization with the maximum object displacement.

We have presented this technique applied to PRC-based HI in [34, 35]. We have pointed out the experimental specifics related to this application. Indeed, the readout is performed when the vibrating object points have a zero velocity, i.e. at the maximum modal displacement. In practice, the opening time has to be long enough in order to obtain a sufficient image intensity at the CCD camera. The duty cycle measures the ratio between the opening time and the vibration period. The quantity of light is proportional to this parameter. If the duty cycle is increased, a higher luminous level reaches the CCD but, in counterpart, one integrates interferograms of the moving object before and after its maximum displacement. As a consequence, the contrast of the fringes decreases because the object is partly seen moving. We have analyzed the errors coming from the phase calculation as a function of the duty cycle. Also we have shown an original technique to deduce this error from the measurements. After correction, the final accuracy is limited by the external perturbations, as for the static displacement measurements, say $\lambda/40$ RMS. In practice, duty cycles of 12% to 16% are used and the object has to be set closer to the holographic head. With a YAG laser (532 nm) emitting 490 mW, we were able to observe very good interferograms on a 23 cm $\times$ 23 cm aluminum plate.

With this technique, we have recently studied the vibration modes of a turbine (10 cm high and 6 cm wide). It is clamped on its base and vibrated by a piezoelectric translator. Figure 10 shows the modes appearing at two excitation frequencies.

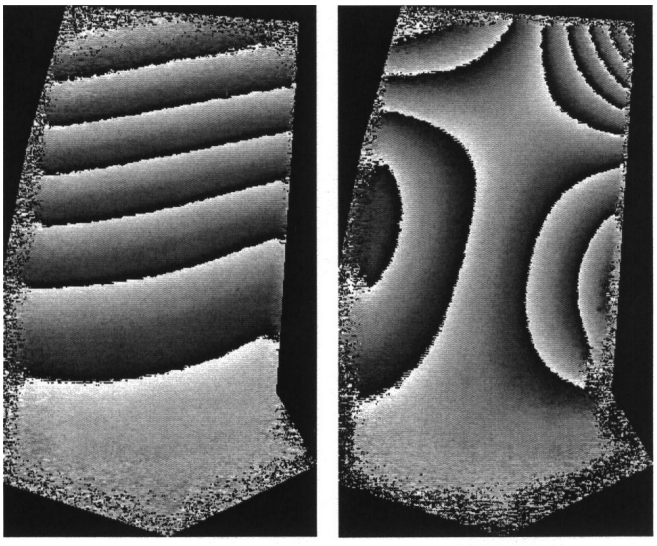

Fig. 10. Two vibration modes of a turbine blade stimulated by a piezoelectric translator

5 Conclusions

The aim of this work was the development of a transportable holographic interferometer using a photorefractive crystal. The instrument specifications are that it has to allow the observation of opaque scattering objects with medium to large dimensions (a typical 50 cm $\times$ 50 cm observed area was assumed), it has to be simple to use, it has to easily give interpretable results, and it has to be sufficiently versatile to be adapted in different kind of applications.

First, we have shown that the configuration of diffraction anisotropy associated with the real-time holographic interferometry technique is the best suited from several points of view. Indeed it can be adapted to a large number of applications and it is compliant with the instrumental specifications, mainly the ease of use and the possibility of large-objects visualisation. A preliminary set-up applying this technique has been shown and was useful in order to point out the aspects that had to be optimized.

Second, a broad study has been carried out along three axes of work. The first axis concerns the comparison of two imaging systems. It is shown that an image-holography design minimizes the necessary laser power and allows us to obtain good quality interferograms on 50 cm $\times$ 50 cm surfaces on the basis of a typical laser power of 400 to 500 mW. The second axis consists in the experimental comparison of the holographic performances of several large-size sillenite crystals, in order to select the best one for the instrument. Here we have chosen a copper-doped BGO crystal but it cannot be concluded necessarily that this species is the best one. Simply this sample gave the most satisfying response as a function of criteria appropriate to HI. The third axis concerns the study of two phase-quantification methods. The first one is the temporal phase-shifting. An original error calculation has been shown that takes into account the dynamic behaviour of the photorefractive crystal, which we called the photorefractive error. It was shown that under practical working conditions, it does not affect the accuracy which is limited to $\lambda/40$ RMS in the object displacement, mainly due to the external perturbations. The second quantification method is the Fourier filtering of the interferogram with a spatial carrier. The principal difficulty arises in the physical introduction of the carrier fringe pattern in the interferogram. Usual techniques cannot be used due to angular selectivity of the crystal. We have shown that the carrier addition is possible by translating the object illumination source.

With the breadboard instrument, we have shown numerous applications, ranging in three categories: static, dynamic (non-vibratory), and vibratory displacements. Our originality is situated at several levels. First, we have presented particular techniques necessary for the observation of the various kinds of phenomena and that were not yet considered with sillenite crystals: the sequential and stroboscopic readouts. Second, we have associated with these techniques a phase-quantification technique that is the most suited. Third, most studied objects are the largest ever observed with a photorefractive interferometer. It must be outlined that the instrument can be adapted in a simple way from one application to another one. Our objectives are then completely fulfilled.

The whole study leads to a transportable optimized holographic interferometer breadboard, allowing quantitative displacements measurement with a high accuracy on medium to

large scattering objects and adaptable to a large range of applications.

Present works are in progress for the improvement of this instrument. First, the use of Q-switched pulsed YAG lasers allowing measurements in perturbed environments, as well as the observation of fast phenomena. Second, the use of optical fibers replacing some optical elements rendering the holographic head more compact and lightweight and increasing its flexibility.

Acknowledgements. This work is supported by the General Direction of Technologies, Research and Energy at the Ministry of Walloon Region of Belgium.

References

1. P.K. Rastogi (Ed.): *Holographic Interferometry: Principles and Methods* (Springer, Berlin, Heidelberg 1994)
2. T. Kreis: *Holographic Interferometry: Principles and Methods* (Akademie, Berlin 1996)
3. P. Günter, J.P. Huignard (Eds.): *Photorefractive Materials and their Applications I, Fundamental Phenomena* (Springer, Berlin, Heidelberg 1988)
4. M.P. Petrov, S.I. Stepanov, A.V. Khomenko: *Photorefractive crystals in coherent optical systems* (Springer, Berlin, Heidelberg 1991)
5. P. Günter, J.P. Huignard (Eds.): *Photorefractive materials and their applications II, Survey of applications* (Springer, Berlin, Heidelberg 1989)
6. D.W. Robinson, G.T. Reid (Eds.): *Interferogram Analysis: Digital Fringe Pattern Measurement Techniques* (Institute of Physics, London 1993)
7. J.P. Huignard, J.P. Herriau: Appl. Opt. **16**, 1807 (1977)
8. J.P. Huignard, J.P. Herriau, T. Valentin: Appl. Opt. **16**, 2796 (1977)
9. A. Marrakchi, J.P. Huignard, J.P. Herriau: Opt. Commun. **34**, 15 (1980)
10. J.P. Huignard, A. Marrakchi: Opt. Lett. **6**, 622 (1981)
11. J.P. Herriau, J.P. Huignard, A.G. Apostolidis, S. Mallick: Opt. Commun. **56**, 141 (1985)
12. A.A. Kamshilin, M.P. Petrov: Opt. Commun. **53**, 23 (1985)
13. R. Troth, J.C. Dainty: Opt. Lett. **16**, 53 (1991)
14. R.C. Troth, S.L. Sochava, S.I. Stepanov: Appl. Opt. **30**, 3756 (1991)
15. S.V. Miridonov, A.A. Kamshilin, E. Barbosa: J. Opt. Soc. Am. A **11**, 1780 (1994)
16. D. Dirksen, G. von Bally: J. Opt. Soc. Am. B **11**, 1858 (1994)
17. D. Dirksen, F. Matthes, S. Riehemann, G. von Bally: Opt. Commun. **134**, 310 (1997)
18. G. von Bally, F. Rickermann, S. Riehemann: Proc. of JSAP/OSA, Topical Meeting on Photorefractive Materials, Effects and Devices, Chiba, Japan (1997) p. 527
19. F. Rickermann, S. Riehemann, G. von Bally: Opt. Commun. **155**, 91 (1998)
20. B. Pouet, S. Krishnaswamy: Appl. Opt. **35**, 787 (1996)
21. L. Labrunie, G. Pauliat, G. Roosen, J.C. Launay: Opt. Lett. **20**, 1652 (1995)
22. L. Labrunie, G. Pauliat, J.C. Launay, S. Leidenbach, G. Roosen: Opt. Commun. **140**, 119 (1997)
23. S. Nakadate, H. Saito, T. Nakajima: Opt. Acta **33**, 1295 (1986)
24. M.P. Georges, Ph.C. Lemaire: Appl. Opt. **34**, 7497 (1995)
25. M. Georges: PhD Thesis, Université de Liège (1998)
26. M.P. Georges, Ph.C. Lemaire: Proc. SPIE **2652**, 248 (1996)
27. M.P. Georges, Ph.C. Lemaire: Proc. of JSAP/OSA, Topical Meeting on Photorefractive Materials, Effects and Devices, Chiba, Japan (1997) p. 637
28. H. Kogelnik: Bell Syst. Tech. J. **48**, 2909 (1969)
29. M.P. Georges, Ph.C. Lemaire: EOS Topical Meetings Digest **7** on Materials for Non Linear Optics (1996) p. 145
30. M.P. Georges, Ph.C. Lemaire: Proc. SPIE **2782**, 476 (1996)
31. M.P. Georges, Ph.C. Lemaire: Proc. of JSAP/OSA, Topical Meeting on Photorefractive Materials, Effects and Devices, Chiba, Japan (1997) p. 495
32. X. Wang, R. Magnusson, A. Haji-Sheikh: Appl. Opt. **32**, 1983 (1993)
33. J. Mary, Y. Bernard, F. Lefaucheux: J. Opt. Soc. Am. B **7**, 2356 (1990)
34. M.P. Georges, Ph.C. Lemaire: Proc SPIE **3098**, 241 (1997)
35. M.P. Georges, Ph.C. Lemaire: Opt. Commun. **145**, 249 (1998)